17th World Conference on Earthquake Engineering, 17WCEE
Sendai, Japan - September 13th to 18th 2020

NUMERICAL INVESTIGATION OF SRC-RC TRANSFER COLUMNS FOR ENHANCED SEISMIC RESISTANCE

A. Jain[(1)], D.R. Sahoo[(2)], A.K. Jain[(3)]

[(1)] *Research Scholar, Indian Institute of Technology, Delhi, abhishek.jain@civil.iitd.ac.in*
[(2)] *Associate Professor, Indian Institute of Technology, Delhi, drsahoo@civil.iitd.ac.in*
[(3)] *Professor, Indian Institute of Technology, Delhi, akjain@civil.iitd.ac.in*

Abstract

This study investigates the role of embedment of structural steel in transfer columns made of reinforced concrete (RC) and steel reinforced concrete (SRC) along their heights. The transition segments between SRC and RC members in such columns may suffer from severe localized failure under seismic loading condition if these segments are not detailed properly. The design and detailing of SRC-RC transfer columns primarily depend on the embedment length of structural steel, the spacing of lateral ties, and end connections, i.e., base plate and anchor bolts. In this study, a numerical investigation has been conducted on SRC-RC columns under different axial load ratios using a finite element (FE) software ABAQUS. Three-dimensional FE models are subjected to monotonically increasing lateral displacements with constant axial load. The main parameters studied are lateral load-resisting capacity, displacement ductility, and mode of failure of SRC-RC columns. The results of parametric study concluded that 60% of embedment of structural steel with closer tie spacing at the transition location resulted in the better lateral strength to SRC columns but exhibited limited ductility due to sudden shear failure. The precipitous failure of the transfer column was alleviated with provision of base plate and anchor bolts.

Keywords: SRC-RC column; Transfer columns; steel reinforced concrete columns; composite column; finite element modelling; lateral bearing capacity

1. Introduction

Steel-reinforced concrete (SRC) columns are widely used in building structures because of the vast advantages in terms of project economy while keeping the construction time equivalent to a 'pure' steel structure and having fire resistance equivalent to RC columns. A lot of structures are hybrid i.e. having different type of construction material in different stories. Some of the construction projects have lower stories as SRC columns and rest as RC columns due to size restriction as SRC columns can be designed in lower size as compared to RC columns. The alternate arrangement is also feasible in some structures with basements as RC beams and columns whereas upper floors as steel beams with SRC columns where construction speed and ease are of higher importance. One more instance of hybrid structures is the use of SRC columns in the RC structures to alleviate the effect of soft story failure mechanism partially/completely.

The transfer stories are the stories in these hybrid structures, that are partly SRC and partly RC. The extent of SRC column or the embedment length of the structural steel in the RC column is the primary focus of this study. Suzuki *et al.* [1] tested one RC specimen and three SRC-RC specimens with 25%, 50% and 75% embedment length of the structural steel and observed that only the specimen with 75% embedment length could achieve the strength higher than the RC specimen. This showed that the lower embedment length could result in degradation of strength of the RC column itself. Wu *et al* [2] conducted experiments on a RC column and 16 transfer specimens under cyclic lateral loading along with constant axial loads. Test specimens had different embedment lengths and spacings of lateral ties in the region where the structural steel was discontinued, areas of structural steel, and axial load percentages. Test specimens exhibited different failure modes, such as shear-tension, shear-compression and bending failure. Wu *et al.* [3] proposed a formula to determine the minimum extension length and concluded that the deformation capacity and ductility coefficient

was maximum when the embedment length was 60% of the total column length. Huang *et al.* [4] developed a finite element model using computer software ABAQUS to predict the behavior of test specimens. Authors also proposed an expression to predict the shear capacity of SRC-RC transfer columns. However, the predicted shear capacity was found to be smaller than the observed shear strength of SRC-RC columns. Zhang *et al.* [5] simulated the behaviour of transfer columns in Seismostruct software package and concluded that as the embedment increased, the mode of failure was changed to pre-dominantly shear. Similarly, as the axial load ratios were increased beyond 40% of column axail capacity, there was a decrease in the lateral load bearing capacity of the column. This shows that there is a need for the further research on SRC-RC columns to investigate their behavior with varying geometric properties and reinforcement detailing. This paper presents the results of a parametric study conducted on SRC-RC columns numerically.

2. Finite element modelling

Finite element models of SRC-RC columns are developed using a computer software ABAQUS. The details of modelling are discussed in the following sections:

2.1 Geometrical modelling

The concrete and structural steel section were modeled as 8-noded solid elements with reduced integration (C3D8R) and the reinforcement was modelled as truss-elements. All reinforcement bars were modelled with truss element with 2-node linear displacement (T3D2). The mesh size was taken as 25x25x25 mm for all elements. The geometric modelling of SRC-RC members was carried out following the same procedure as adopted by Ellobody and Young [6] and Huang *et al.* [4]. The parameters input in the model are explained in the section.

2.2 Material modelling

The concrete in the specimen was assigned three different material properties in the cross section. Unconfined concrete property to the cover portion, partially confined concrete to the area bound by the lateral ties and highly confined to the area confined by the structural steel.

2.2.1 Steel

The reinforcement and structural steel were modelled with kinematic hardening in the analysis.

2.2.2 Unconfined concrete

Popovic's [7] modified model was used for the material model which was modified further by Collins and Mitchell [8] as:

$$f_c = \frac{f_{co}\lambda\left(\frac{\varepsilon_c}{\varepsilon_o}\right)}{\lambda - 1 + \left(\frac{\varepsilon_c}{\varepsilon_o}\right)^{\lambda d}} \quad \text{where } \lambda = \frac{E_c}{E_c - \left(\frac{f_c}{\varepsilon_o}\right)} \tag{1}$$

$$\text{when d = 1, } \frac{\varepsilon_c}{\varepsilon_o} \le 1,\ d = 0.67 + \frac{f_c}{62} \ge 1,\ \frac{\varepsilon_c}{\varepsilon_o} > 1 \tag{2}$$

E_c is the initial tangent modulus = $5000\sqrt{f_c}$ MPa and $\varepsilon_{co} = 0.002$

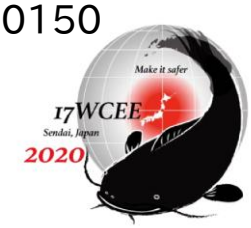

2.2.2 Partially-confined concrete

The model used for simulating the partially confined concrete is as given by Mander *et al.* [9]:

$$f_c = \frac{f_{co} x \left(\frac{\varepsilon_c}{\varepsilon_o} \right)}{r - 1 + x^r} \tag{3}$$

$$\text{where } x = \frac{\varepsilon_c}{\varepsilon_{cc}}, \; r = \frac{E_c}{E_c - E_{sec}} \text{ and } E_{sec} = \frac{f_{cc}}{\varepsilon_{cc}} \tag{4}$$

where f_{cc} and ε_{cc} are calculated as per improved model of Mander *et al.* [9] which was further improved by Denavit *et al.* [10]:

$$f_{cc} = K f_{co} \tag{5}$$

$$\varepsilon_{cc} = \varepsilon_{co}(1 + 5(K - 1)) \tag{6}$$

$$K = 1 + A f_1 \left(0.1 + \frac{0.9}{1 + B f_1} \right) \tag{7}$$

$$A = 6.8886 - (0.6069 + 17.275r)e^{-4.989u} \tag{8}$$

$$B = \frac{4.5A}{5(0.9849 - 0.6306e^{-3.8939u}) - 0.1A} - 5 \tag{9}$$

$$f_1 = \frac{f_{11} + f_{12}}{2 f_{co}} \tag{10}$$

$$u = \frac{f_{11}}{f_{12}}, f_{11} \le f_{12} \tag{11}$$

Where f_{11} and f_{12} is the lateral confining pressure from the lateral ties and reinforcement bars as calculated by Mander *et al.* [8].

2.2.3 Highly-confined concrete

The material model followed was same as the one for partially confined concrete but the value for f_{cc} and ε_{cc} calculated as per the paper from Wei *et al.* [11].

$$f_{1s} = K_s f'_{1s} \tag{12}$$

Where f_{1s} is the lateral confining pressure provided by the steel section.

$f_{11} = f_{12} = f_{1s}$ for lateral loading at the major axis of steel section

$$f'_{1s} = \frac{f_{yst} t^2}{\sqrt{9l^4 + 3l^2 t^2}} \tag{13}$$

$$K_s = \frac{(b_f - t_w)(d_s - 2t_f) - \frac{1}{3}(d_s - 2t_f)^2}{(b_f - t_w)(d_s - 2t_f)} \tag{14}$$

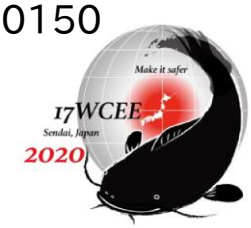

2.2.4 Modeling of tensile behavior of concrete

The fracture energy can be defined as per

$$G_f = G_{fo}\left(f_t\right)^{0.7} \text{ N / mm where } f_t = 0.1 f_{ck} \quad (15)$$

G and G_{fo} ranges from 0.025 to 0.058 for maximum aggregate size 8 mm to 32 mm

The cracking strain for concrete is defined as $\varepsilon_{cr} = f_t / E_o$

$$\varepsilon_1 = \varepsilon_{cr} + \frac{w_1}{l_c} \qquad w_1 = 0.8\frac{G_f}{f_t} \quad (16)$$

$$\varepsilon_u = \varepsilon_{cr} + \frac{w_u}{l_c} \qquad w_u = 3.6\frac{G_f}{f_t} \quad (17)$$

where $l_c = \sqrt[3]{V}$ and $E_o = 5500\sqrt{f_c}$ (18)

2.3 Interaction and constraints

The longitudinal reinforcement and lateral ties were assumed as fully-embedded constraining the translation degrees of freedom and pore pressure degree of freedom to the interpolated values of the corresponding degrees of freedom of the host element. The interactions between concrete section and structural steel were simulated with normal behavior as hard contact and tangential behavior as penalty friction with a coefficient of 0.25.

3. Validation of FE Models

The validation of finite element models was carried out by comparing the test results [1, 2]. Tables 1 and 2 summarizes the material and geometrical details of test specimens.

Table 1 – Details of the material in the papers (MPa)

Item	S3-60 Specimen [1]	SRC 6-2 Specimen [2]
Longitudinal reinforcement	755	358.3
Structural steel	228	292.7
Lateral ties	363	292.7
Concrete cube strength	25.9	59.1

Table 2 – Details of the geometry in the papers (in mm)

Item	S3-60 Specimen [1]	SRC 6-2 Specimen [2]
Section size (mm)	275 x 275	160 x 220
Structural steel dimension (mm)	204 x 12 x 200 x 12	140 x 5.5 x 80 x 9.1
Reinforcement bars	8 nos. – 19 φ	4 nos. – 16 φ
Clear length of the specimen (mm)	1200	1000
Axial load ratio	0.15	0.2
Embedment length (mm)	600	600
Spacing of lateral ties (mm)	10φ@120 c/c	6.5φ@48 c/c

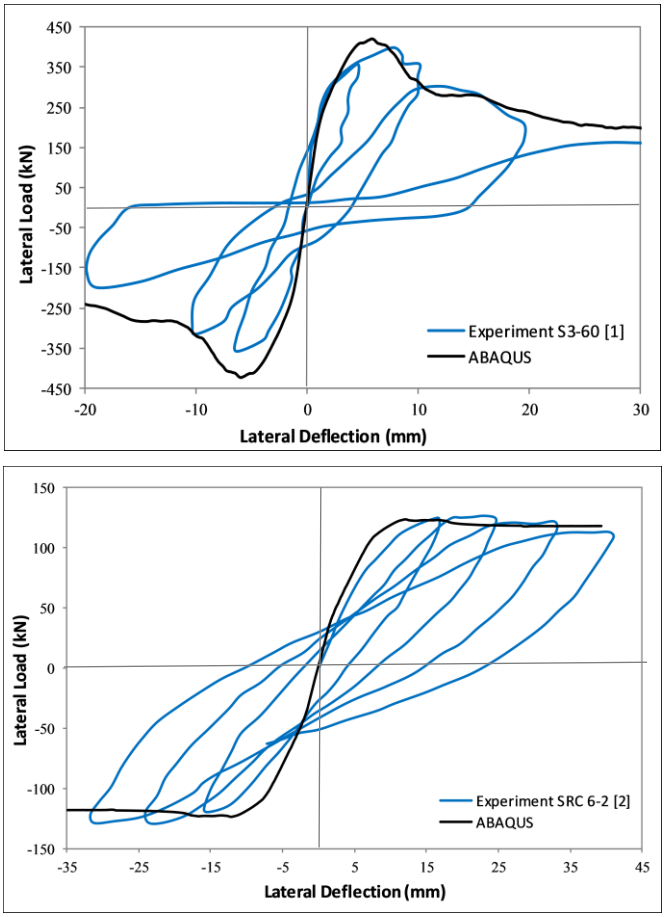

Fig. 1 – Failure mechanism comparison between experiment and ABAQUS simulation from research conducted by [1] (left) and [2] (right)

As shown in Fig. 1 and Fig. 2, a fair match was observed with backbone curve and failure mechanism of the test specimen and the numerical model. While a predominantly shear failure was observed in S3-60 [1], a flexural shear failure was observed for the SRC 6-2 specimen [2]. SRC 6-2 crack pattern were not shown mentioned, the failure patters for another specimen S6-4 [2] were matched to show the validation of the ABAQUS model.

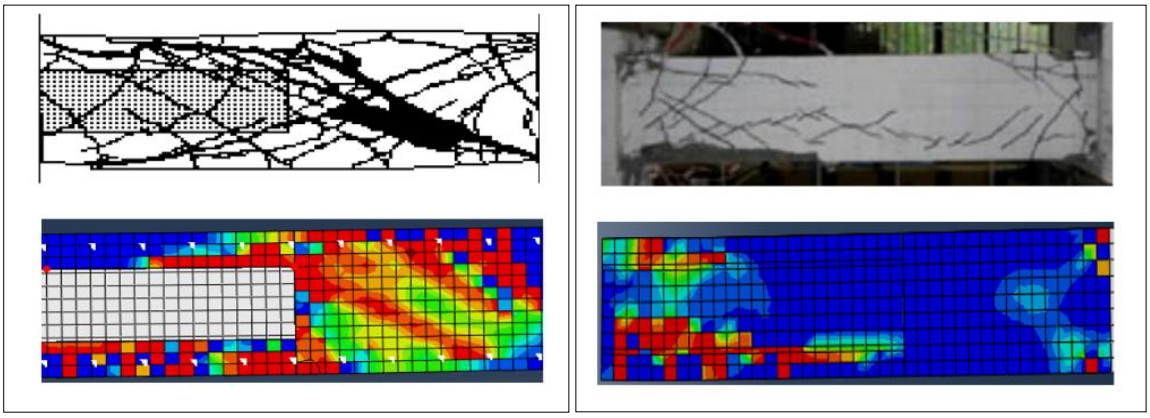

Fig. 2 – Failure mechanism comparison between experiment and ABAQUS simulation from research conducted by [1] (left) and [2] (right)

4. Parametric Study

4.1 Modelling

The validated finite element model was used in the parametric study. The geometry of test specimen was kept same as used in the previous study [2]. The boundary conditions were modified to strictly restrict rotation on both ends as shown in Fig. 3. The parameters studied in the model were structural steel embedment, axial load ratio and end conditions like base plate and anchors. The lateral ties were kept closer at the truncation zone. The specimens were tested for axial load ratio of 20%, 40 and 50%. The embedment length percentage was ranged from 30% - 60% for both of axis. Few simulations were carried out with steel section culminating in the RC part with base plate and anchors. The anchors were modelled as steel elements which were simulated with the embedment constraint in the RC portion.

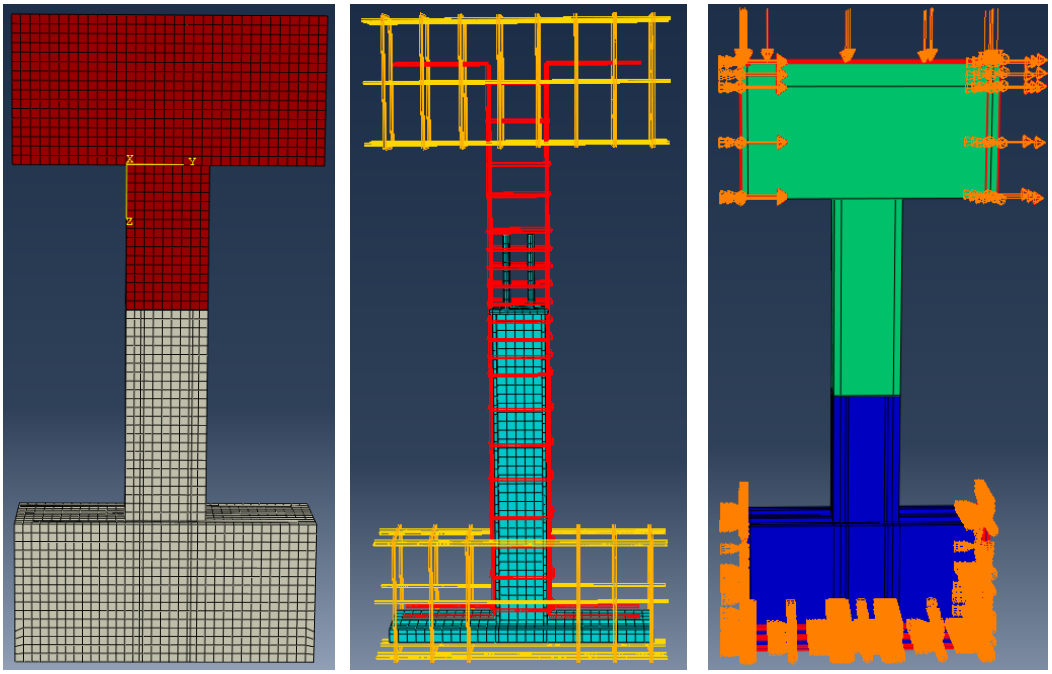

Fig. 3: Hybrid Specimen Geometry (left), Reinforcement and structural steel arrangement (center) & boundary conditions (right)

Like the structural steel section, penalty friction interaction was applied between base plate and concrete part. The details of geometric loading properties of numerical models are shown in Table 3. Furthermore, specimen with pure RC and SRC section throughout the length of the section was simulated as well to get a baseline for the maximum capacity the section can achieve. The numerical model specimens are referred to XX-Hyb-YY, where XX denotes the percentage embedment of structural steel in transfer column and YY denotes the percentage of axial load.

4.2 Analysis

The lateral force capacity and ductility of the specimen were studied and tabulated in table 3. The ductility was defined as Δ_u/Δ_y where Δ_u and Δ_y are ultimate and yield lateral displacement.

Table 3: Specimen for Parametric Study with results

Models	Embedment Length (%)	Axial load (%)	Detailing	Lateral Force Capacity (kN)	Ductility
RC-20	-	20		124	6.98
30-Hyb-20	30	20		147	4.30
40-Hyb-20	40	20		149	4.50
40-Hyb-20-BP	40	20	Base plate & Anchors	149	7.46
50-Hyb-20	50	20		150	4.50
60-Hyb-20	60	20		149	8.94
60-Hyb-20-BP	60	20	Base plate & Anchors	153	8.11
SRC-20	-	20		165	10.15
RC-40	-	40		149	3.66
30-Hyb-40	30	40		167	2.83
40-Hyb-40	40	40		162	3.20
40-Hyb-40-BP	40	40	Base plate & Anchors	158	3.98
50-Hyb-40	50	40		166	4.14
60-Hyb-40	60	40		165	4.57
60-Hyb-40-BP	60	40	Base plate & Anchors	169	4.16
SRC-40	-	40		177	6.08
RC-50	-	50		147	2.89
30-Hyb-50	30	50		163	2.99
40-Hyb-50	40	50		163	3.00
50-Hyb-50	50	50		151	2.55
60-Hyb-50	60	50		163	3.17
SRC-50	-	50		124	6.98

Figure 4 shows the lateral force-displacement response of SRC-RC columns for 20%, 40% and 50% axial load levels. It was observed that the lateral capacity of all the specimen were higher than the pure RC specimen. However, the ductility of the hybrid specimen did not follow the same pattern. All the specimen with embedment less than 60%, had the ductility less than pure RC specimen. Furthermore, a sudden degradation was seen for these specimens indicating shear predominant failure. The ductility of 40-Hyb-20-BP and 40-Hyb-40-BP was higher than the RC specimen. Increase in the axial load ratio from 20% to 40% led to increase in lateral bearing capacity and understandably, decrease in ductility.

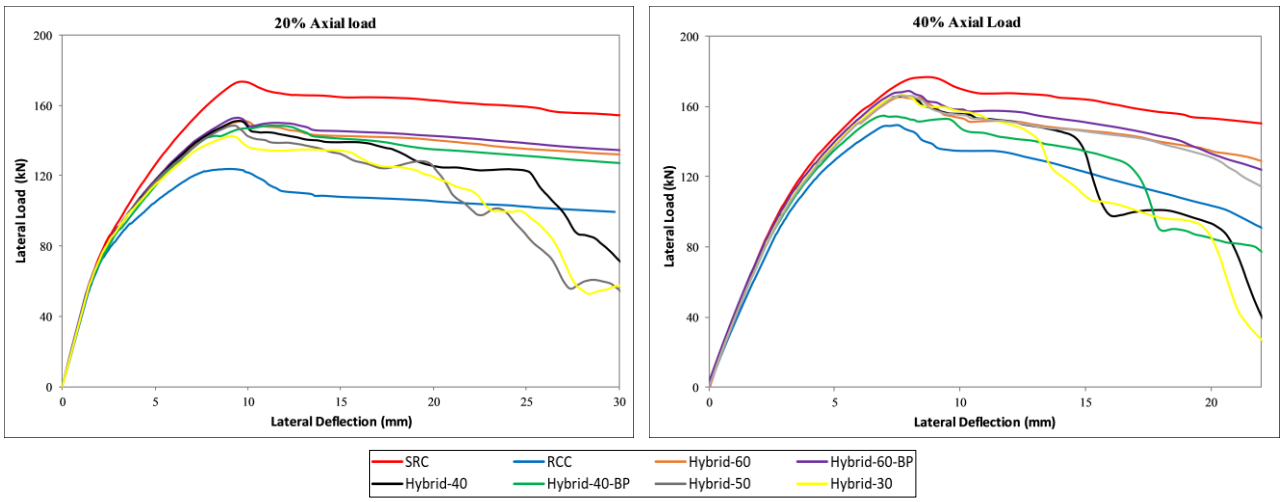

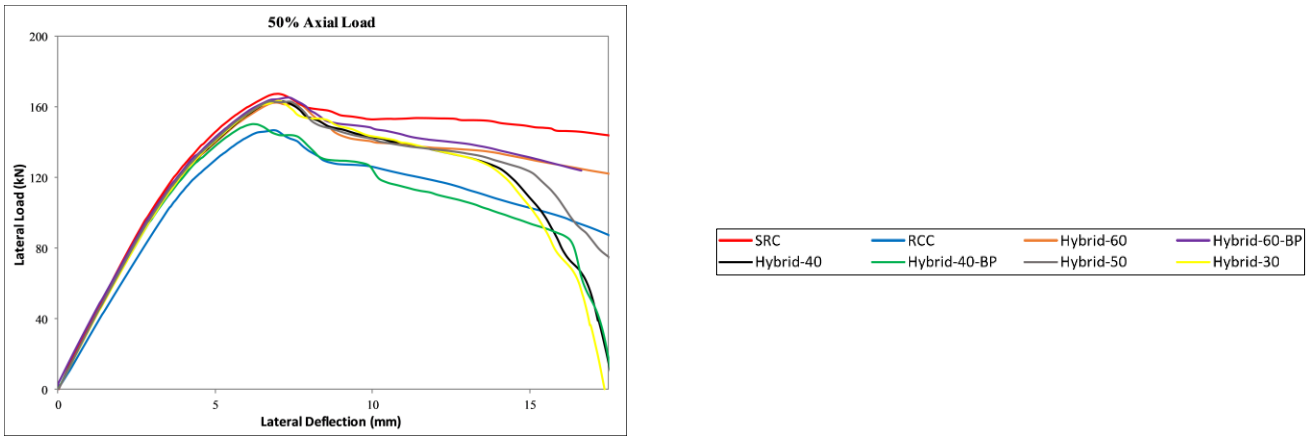

Fig. 4: Comparison of load-displacement response of parametric study on SRC-RC columns

5. Conclusions

The following conclusions can be drawn from this study:

- The validation of the ABAQUS model was conducted by comparing the experiment cyclic curves with backbone curve obtained from the simulation. The failure mechanism also reasonably matched.
- It was observed that 60% embedment of structural steel had lateral strength and ductility higher than the pure RC specimen for all the axial load ratio. It is of importance because embedment of steel should not make the RC section weak.
- Axial load ratio of the transfer column should be restricted to 40% to avoid brittle failure in the section
- The addition of anchor bolts and base plate significantly increased the performance for the 40% embedment length specimen making it as a valid specimen for employing in the structure and same must be studied further with experiments.

6. References

[1] Suzuki H, Nishihara H, Matsuzaki Y, Minami K (2000): Structural performance of mixed member composed of steel. *12WCEE,* Auckland, 1–8.

[2] Wu K, Xue J, Zhao H (2013): Failure mechanism and bearing capacity of transfer columns in SRC-RC hybrid structures. *European Journal of Environmental and Civil Engineering* 17, 205–228.

[3] Wu K, Xue J, Nan Y, Zhao H (2018): Analysis on Extension Length of Shape Steel in Transfer Columns of SRC–RC Hybrid Structures. *International Journal of Steel Structures* 18(3), 910–23.

[4] Huang W, Zhou Z, Liu J (2017): Analytical deformation characteristics and shear capacity of SRC-RC transfer columns. *Journal of Constructional Steel Research*, 138, 692–700.

[5] Zhang H, Cao P, Wu K, Xu C, Ren L (2019): Lateral Bearing Capacity and Stiffness Calculation Method of SRC-RC Columns. *KSCE Journal of Civil Engineering*, 1–17.

[6] Ellobody, E. and Young, B., (2011): Numerical simulation of concrete encased steel composite columns. *Journal of Constructional Steel Research*. *67*(2): 211-222.

[7] Popovics, S., (1973): A numerical approach to the complete stress-strain curve of concrete. *Cement and concrete research*, *3*(5), 583-599.

[8] Collins, M.P., Mitchell, D. and Macgregor, J.G., (1993): Structural design considerations for high-strength

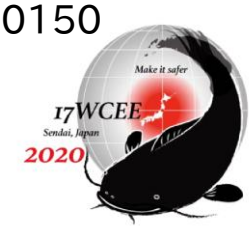

concrete. *Concrete international*, *15*(5), 27-34.

[9] Mander, J.B., Priestley, M.J. and Park, R., (1988): Theoretical stress-strain model for confined concrete. *Journal of structural engineering*, *114*(8):1804-1826.

[10] Denavit, M.D., Hajjar, J.F. and Leon, R.T. (2011). Seismic behavior of steel reinforced concrete beam-columns and frames. In *Structures Congress 2011*, 2852-2861.

[11] Wei, H., Jiang, Q. and Zhi, Z., (2016): Numerical simulation of the seismic performance of steel reinforced concrete columns by considering the lateral confining pressure. *Engineering mechanics*. *33*(5), 157-165.

[12] Popovics, S., (1973): A numerical approach to the complete stress-strain curve of concrete. *Cement and concrete research*, *3*(5), 583-599.

[13] Dassault Systemes (2010): ABAQUS documentation and user manual. Version 6.10

